# Hydrodynamic performance characterisation of a tidal energy generation system buoyancy assembly using CFD

Lawrence S. H. Lai, Nathaniel C. Hayes

***Abstract*—The TidGen 2.0 Power System is an electricity generation system which functions by harnessing energy from tidal currents. The current work looks to assess the hydrodynamic characteristics of its buoyancy assembly using computational fluid dynamics. The numerical simulation is performed using a transient k-epsilon Reynolds-averaged Navier-Stokes numerical scheme. The main set of simulations was done with a simplified geometry model consisting of an elongated cylindrical form. Variation in flow attack angles was simulated to represent system pitch at the prevalent operational current flow speed. Its effect on the lift coefficient was monitored to ensure the buoyancy assembly is not susceptible to periodic vortex shedding, which is a pre-cursor to vortex-induced vibrations (VIV). VIV would negatively impact component structural strength and fatigue life. The simplified geometry simulations show in-line drag to be low in the range 0.28 to 0.31 for the 0 to 5 deg. attack angle considered. However, vortex shedding was seen to be periodic which may present a VIV risk. Therefore further investigation was performed using a more detailed buoyancy assembly model with surface features like flanges and corrugations. It was shown the base in-line drag coefficient increased from 0.28 to 0.36. The VIV propensity was assessed to be adequately mitigated and not be a significant concern. Overall, the in-line drag is shown to be suitably low with minor risk of VIV occurring and is deemed suitable for the purposes of the TidGen 2.0 system implementation.***

***Keywords*—buoyancy, hydrodynamics, computational fluid dynamics, vortex-induced vibration, tidal energy, renewable energy.**

ID Number 1212, Track TDD. This work was produced through collaboration between Ocean Renewable Power Company and Trelleborg Offshore.

Lawrence S. H. Lai is a Product Development Engineer with Trelleborg Offshore US situated at 1902 Rankin Road, Houston, TX, 77073 U.S.A. (e-mail: lawrence.lai@trelleborg.com)

Nathaniel C. Hayes is a Lead Engineer for Autonomous Systems with Ocean Renewable Power Company situated at 254 Commercial St., Suite 119B, Portland, Maine, 04101, U.S.A. (e-mail: nhayes@orpc.co)

## I. Introduction

THE TidGen 2.0 Power System is an electricity generation system which functions by harnessing energy from tidal currents. A front-view diagram of the system is shown in Figure 1. It consists of a moored turbine assembly that is kept in tension by a buoyancy system which has an elongated cylinder profile. The current work looks to define the hydrodynamic characteristics of the buoyancy assembly with Computational Fluid Dynamics (CFD) using Siemens StarCCM+. This is to confirm the design efficacy in terms of having low in-line drag which in turn minimises lateral and pitching deflection of the entire system.

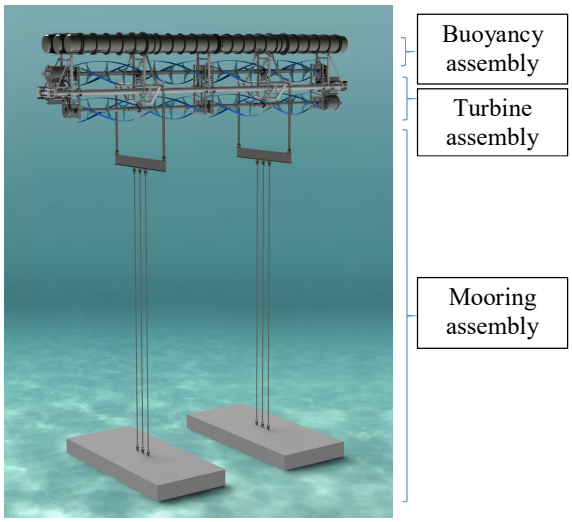


Fig. 1. Front view diagram of the TidGen 2.0 system showing the three main system assemblies of buoyancy, turbine and mooring. The buoyancy assembly is the focus of this hydrodynamics assessment.

The CFD methodology employed uses a transient Reynolds-averaged Navier-Stokes (RANS) model and simulates only the buoyancy assembly. This is so a better understanding of the hydrodynamic behaviour for just the buoyancy component can be determined. A simplified geometry is employed to determine the key hydrodynamic characteristics of the buoyancy assembly shape being an elongated cylinder. A more detailed model will also be analysed to ensure the simplified

  

geometry findings are representative of the actual buoyancy assembly.

The main objective is an evaluation of the overall drag loading on the buoyancy component and some indication of vortex-induced vibration (VIV) propensity. This would then be the basis to inform on the overall system suitability of this component in the TidGen 2.0 system.

### A. Abbreviations and acronyms

Listed in this section are the abbreviations and acronyms used throughout this paper.

| | |
|---|---|
| ORPC | Ocean Renewable Power Company |
| TO | Trelleborg Offshore |
| VIV | Vortex-induced vibration |
| CFD | Computational fluid dynamics |
| RANS | Reynolds-averaged Navier-Stokes |

## II. Mathematical Formulae

### B. Governing Equations

The numerical solution is based on the approach proposed by [1]. This transient turbulence model solves for the turbulent kinetic energy $k$ and turbulent dissipation rate $\varepsilon$ ($k$-$\varepsilon$), normalized (reduced) wall-normal stress $\varphi$ and elliptic blending to capture the suitable near-wall conditions represented by the elliptic blending factor $\alpha_b$. The transport equations for the four variables $k$, $\varepsilon$, $\varphi$ and $\alpha_b$ are given by

$$\frac{\partial}{\partial t}(\rho k) + \nabla \cdot \left[\rho k\left(\bar{v} - v_g\right)\right] = \nabla \cdot \left[\left(\frac{\mu}{2} + \frac{\mu_t}{\sigma_k}\right)\nabla k\right] + P_k - \rho(\varepsilon - \varepsilon_0) + S_k \tag{1}$$

$$\frac{\partial}{\partial t}(\rho \varepsilon) + \nabla \cdot \left[\rho \varepsilon\left(\bar{v} - v_g\right)\right] = \nabla \cdot \left[\left(\frac{\mu}{2} + \frac{\mu_t}{\sigma_\varepsilon}\right)\nabla \varepsilon\right] + \frac{1}{T_\varepsilon} C_{\varepsilon 1} P_\varepsilon - C_{\varepsilon 2}\left(\frac{\varepsilon}{T_\varepsilon} + \frac{\varepsilon_0}{T_0}\right) + S_\varepsilon \tag{2}$$

$$\frac{\partial}{\partial t}(\rho \varphi) + \nabla \cdot \left[\rho \varphi\left(\bar{v} - v_g\right)\right] = \nabla \cdot \left[\left(\frac{\mu}{2} + \frac{\mu_t}{\sigma_\varphi}\right)\nabla \varphi\right] + P_\varphi + S_\varphi \tag{3}$$

$$\nabla \cdot (L^2 \nabla \alpha_b) = \alpha_b - 1 \tag{4}$$

Where
$C_{\varepsilon 1}$, $C_{\varepsilon 2}$, $\sigma_k$, $\sigma_\varepsilon$, $\sigma_\varphi$ and are model coefficients
$P_k$, $P_\varepsilon$, and $P_\varphi$ are production terms
$S_k$, $S_\varepsilon$, and $S_\varphi$ are the source terms
$\bar{v}$ is the mean velocity
$v_g$ is the reference frame velocity

The turbulent viscosity $\mu_t$ is calculated as

$$\mu_t = \rho C_\mu \varphi k \max\left(T, \frac{C_T}{\sqrt{3} C_\mu \varphi s}\right) \tag{5}$$

Where
$\rho$ is the fluid density
$C_\mu$ and $C_T$ are model coefficients
$S$ is the mean strain rate tensor modulus
$T$ is the turbulent time-scale

$$T = \sqrt{T_e^2 + C_t^2 \frac{\upsilon}{\varepsilon}} \tag{6}$$

Where
$T_e = k/\varepsilon$ is the fluid density
$C_t$ is a model coefficient
$\upsilon$ is a kinematic viscosity

$L_s$ is the length scale calculated as

$$L_s = C_L \sqrt{T_e^3 + C_\eta^2 \sqrt{\frac{\upsilon^3}{\varepsilon}}} \tag{7}$$

Where
$C_L$ and $C_\eta$ are model coefficients

The CFD model coefficients are specified in Table I.

TABLE I
CFD MODEL COEFFICIENTS USED IN NUMERICAL SETTINGS

| Parameter | $C_{\varepsilon 1}$ | $C_{\varepsilon 2}$ | $C_{\varepsilon 3}$ | $C_\mu$ | $C_L$ |
|---|---|---|---|---|---|
| Value | 1.44 | 1.83 | 1.00 | 0.22 | 0.164 |

| Parameter | $C_\eta$ | $C_T$ | $\sigma_k$ | $\sigma_\varepsilon$ | $\sigma_\varphi$ |
|---|---|---|---|---|---|
| Value | 75.0 | 1.0 | 1.0 | 1.5 | 1.0 |

### C. Hydrodynamic Performance Assessment Method

Hydrodynamic behaviour is characterised in terms of the directional drag coefficients $C_{di}$ where the subscript $i$ refer to the three translational directions of in-line with flow $x$, horizontal cross-flow $y$ and vertical or lift $l$. The translation direction convention is shown in Figure 3 which also shows the fluid domain and bluff body. The equation for $C_{di}$ is given by

$$C_{di} = \frac{F_{di}}{\rho V_\infty^2 D} \tag{8}$$

Where $F_{di}$ are the hydrodynamic forces in their respective translation directions, $\rho$ is the fluid density, $V_\infty$ is the free-stream velocity and $D$ is the nominal bluff body diameter $D_b$. Given that the simulations are transient, the values for $F_{di}$ are time-varying. As such, the resultant output is presented in terms of the average

value $C_{di,avg}$ or root-mean-square variation $C_{di,rms}$ The definitions for these terms are respectively

$$C_{di,avg} = \frac{\sum_{t=1}^{n} C_{di,t}}{n} \tag{9}$$

$$C_{di,rms} = \sqrt{\frac{\sum_{t=1}^{n} \left(C_{di,t} - C_{di,avg}\right)^2}{n}} \tag{20}$$

Where $n$ is the number of constant delta time incremental samples.

A range of flow speeds prevalent in the offshore environment is analysed and is represented by the Reynolds number *Re*, which is

$$Re = \frac{\rho V_\infty D}{\mu} \tag{31}$$

Where $\mu$ is the fluid dynamic viscosity.

## III. CFD Model Setup

### *D. Geometry, Boundary Conditions and Mesh*

A diagram of the buoyancy assembly is shown in Figure 2. The assembly consists of six steel aircans affixed together to form an elongated cylindrical form.

A simplified geometry as shown in Figure 3 is generated for the main set of CFD simulations. The intent of this simplified model is to understand the effect of the overall elongated cylindrical form of the buoyancy assembly. This geometry model is the main model used for the majority of simulations in this paper.

The main boundary conditions are also shown in Figure 3. The domain and bluff body (buoyancy assembly) boundary specifications are listed below.

- Inlet: A constant, uniform velocity is applied across the entire inlet, representing the upstream inward flow
- Outlet: A zero (ambient) outlet pressure condition is applied at the outlet face with no velocity condition imposed on the face
- Bluff body: A rigid bluff body representing half of the buoyancy assembly is simulated within the fluid domain. The bluff body is solid and has no-slip surface conditions
- Symmetry planes: The four surface boundaries connecting the inlet and outlet faces are imposed as symmetry planes with slip (no shear) conditions. One of the symmetry planes is in contact with the buoyancy component which is also its symmetry split-line.

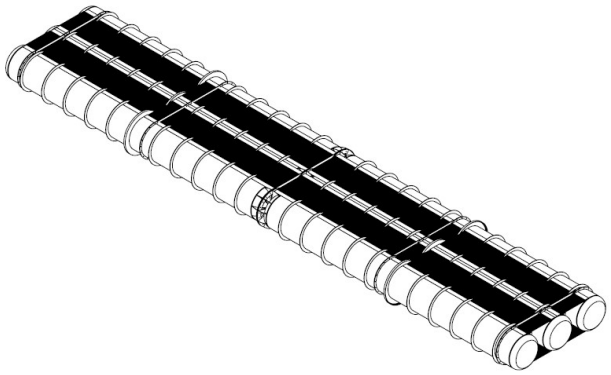

Fig. 2. Detailed diagram of TidGen 2.0 buoyancy assembly consisting of six aircans.

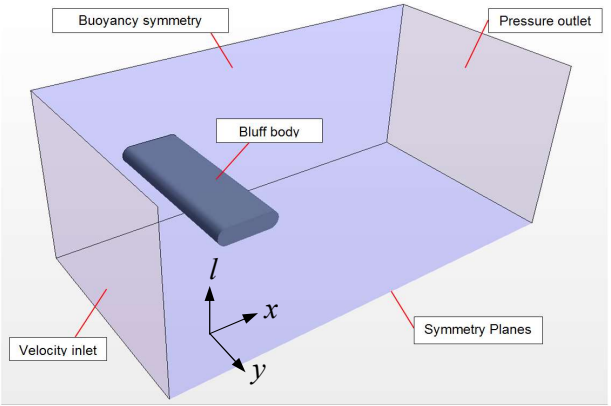


Fig. 3. CFD model of the simplified elongated cylindrical form for the buoyancy assembly. Half of the actual geometry is modelled along its mid symmetry plane for computational efficiency.

A more detailed CFD model of the buoyancy assembly with local surface features (flanges, corrugated plates, reinforcement joists, etc.) is also analysed as shown in Figure 4. Only a single simulation was performed using this detailed geometry to compare and confirm the simplified model's validity.

The main CFD domain dimension labels are shown with the front and side views in Figure 5 and the relevant dimensional values listed in Table I. The 'length' of the buoyancy is termed with the notation '*W*' because although it relates to the longer dimension of the buoyancy component, from the fluid domain's perspective it relates to the fluid domain's width. Similarly the buoyancy 'width' is denoted '$L_b$' as it relates to the fluid domain's length. The fluid domain upstream length $L_{up}$ is the length from the inlet to the leading buoyancy circle center and $D_b$ is the vertical 'thickness' or rounded edge diameter of the buoyancy assembly.

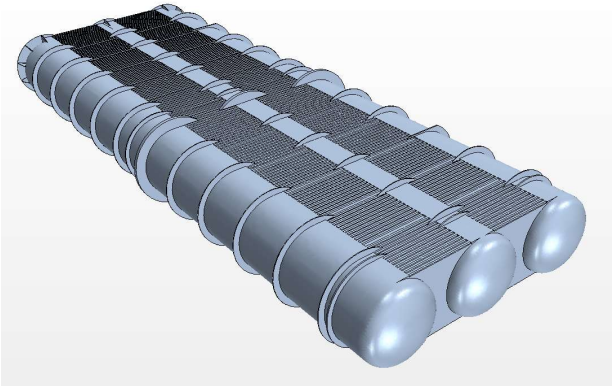

Fig. 4. CFD model of the detailed buoyancy assembly to confirm validity of the simplified CFD model, used for a single simulation only. Only half of the assembly is simulated due to the symmetry plane.

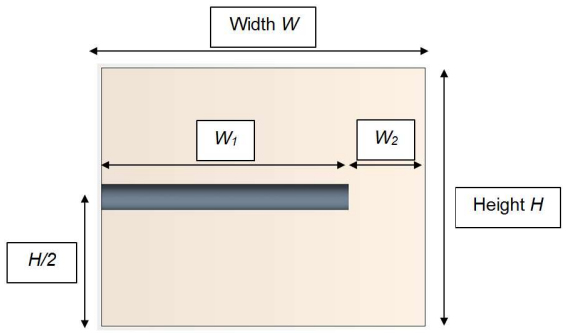


(a) Front view

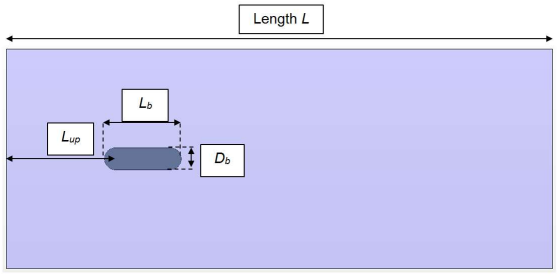


(b) Side view

Fig. 5. Fluid domain and buoyancy assembly dimensional designations.

TABLE I
BUOYANCY AND FLUID DOMAIN DIMENSIONAL PARAMETERS

| Symbol | Dimensional Parameter | Value |
|---|---|---|
| $D_b$ | Bluff body diameter | 1.68 m |
| $W_b$ | Bluff body length | 32.08 m |
| $L_b$ | Bluff body depth | 5.88 m |
| $L$ | Fluid domain length | 25 $D_b$ |
| $L_{up}$ | Fluid domain upstream length | 5 $D_b$ |
| $H$ | Fluid domain height | 10 $D_b$ |
| $W$ | Fluid domain total width | 12.6 $D_b$ |
| $W_1$ | Bluff body width | 9.6 $D_b$ |
| $W_2$ | Fluid domain side clearance width | 3.0 $D_b$ |

The CFD model fluid domain mesh is shown in Figure 6 with the overall domain consisting of polyhedral mesh. Mesh refinement is applied when approaching the bluff body and downstream of the flow to capture the vortex shedding behaviour. The fluid-wall boundary has prismatic polyhedral mesh to capture wall boundary effects. Domain sensitivity is performed by increasing the domain to double the size, i.e. 2$L$, 2$L_{up}$, 2$H$ and 2$W$ and showed little variation in the final control outputs (i.e. transient hydrodynamic drag values).

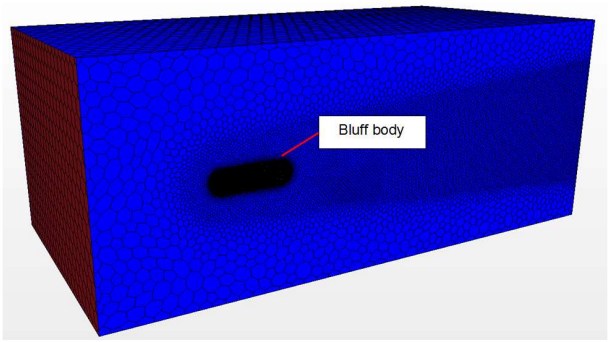


Fig. 6. CFD fluid domain mesh with mesh refinement near the bluff body wall and downstream of fluid flow to resolve the wake behaviour.

### E. *Environment Conditions and Environmental Properties*

The relevant flow velocities for this system are listed in Table II. For the purpose of this study, the operational and extreme (ultimate limit) current conditions are considered. The corresponding $Re$ values are also provided and both flow speeds are within the highly turbulent flow regime. $Re$ uses $D_b$ as the characteristic length.

The fluid considered is water with properties listed in Table III. The specific seawater properties dependent on salinity and temperature have not been used for simplicity as the effect on the controlling parameter $Re$ is minor. Furthermore the relationship of $C_d$ and $Re$ due to this variation is expected to be insensitive. The surface roughness selected is relatively smooth with $k = 5 \times 10^{-5}$ m. This is level of surface roughness is similar to new, uncoated steel as per DNV-RP-C205 [2].

The TidGen is a moored system and as such is able to pitch due to ocean current action. Therefore it is important to analyse pitch effect in terms of varying the flow attack angle. Orientation of the buoyancy assembly relative to horizontal flow direction (left to right) is shown in Figure 7. The default position is with attack angle $\alpha$ at 0 deg. or lateral along the flow direction (left to right). A maximum $\alpha$ = 5 deg. pitch variation with 1 deg. increments is considered.

TABLE II
FLOW CONDITIONS AND VELOCITY MAGNITUDES

| Flow Condition | Velocity Magnitude $V_\infty$ (m/s) | Reynolds number $Re$ |
|---|---|---|
| Operational | 2.25 | $3.8 \times 10^6$ |

TABLE III
FLUID PROPERTIES AND VALUES

| Parameters | Reynolds number $Re$ |
|---|---|
| Density $\rho$ | $1 \times 10^3$ kg/m$^3$ |
| Dynamic viscosity $\mu$ | $1 \times 10^{-3}$ Pa.s |
| Surface roughness $k$ | $5 \times 10^{-5}$ m |

(a) Default base case with $\alpha = 0$ deg.

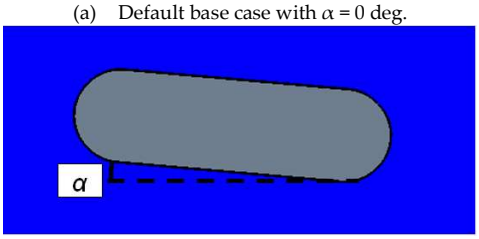


(b) Maximum operational pitch condition with $\alpha = 5$ deg.

Fig. 7. Side view illustrating buoyancy orientation with different flow attack angles $\alpha$ considering fluid flow from left to right.

## IV. RESULTS AND DISCUSSION

### F. Simplified Geometry Hydrodynamic Characteristics

The time-averaged in-line $C_{dx,avg}$ and cross-flow $C_{dy,avg}$ drag coefficients are shown in Figure 8 and 9 respectively. There is little change in $C_{dx,avg}$ from 0.28 to 0.31 with the change of $\alpha$ angle from 0 to 5 deg. There is a linear increase in $C_{dy,avg}$ from 0 to 1.43 with the increase of $\alpha$ angle. This is beneficial as it further tensions the TidGen assembly which makes it upright, as opposed to being further deflected laterally downstream. Though, additional lift loading has to be factored in when considering the strength limits of the mooring lines.

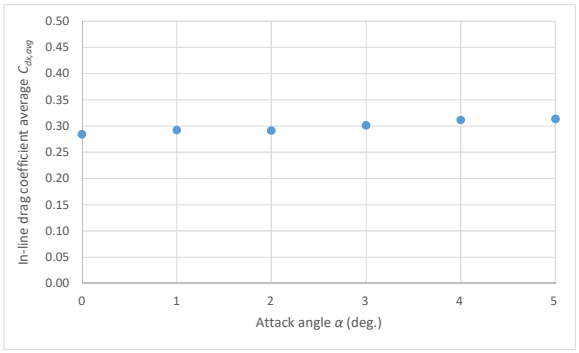


Fig. 8. Time-averaged in-line drag coefficient $C_{dx,avg}$ for different attack angles $\alpha$.

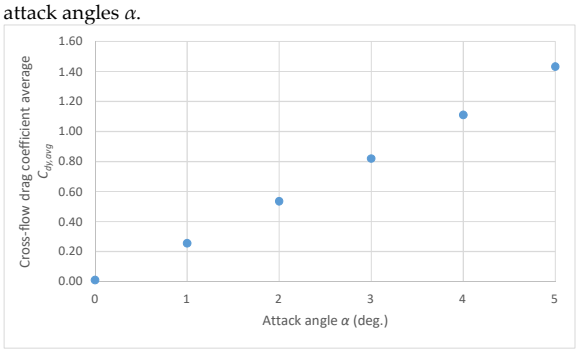


Fig. 9. Time-averaged cross-flow drag coefficient $C_{dy,avg}$ for different attack angles $\alpha$.

The $C_{dy,rms}$ which is a measure of VIV propensity in Figure 10 shows there is a non-zero probability of VIV occurring considering the uniform, elongated cylindrical shape. In comparison, it has been seen for a circular cylinder $C_{dy,rms} > 0.2$ is considered to have significant VIV risk based on [3].

Figure 11 shows the perspective view of the fluid domain with a limited set of streamlines for flow in the vicinity of the bluff body at the two extreme $\alpha$ angles. The streamlines have velocity magnitude colour contours. Consistent over all $\alpha$ angles, it can be seen the downstream flow produces periodic oscillations. There is no perceptible difference in the streamline flow behaviour to distinguish between different $\alpha$ angles.

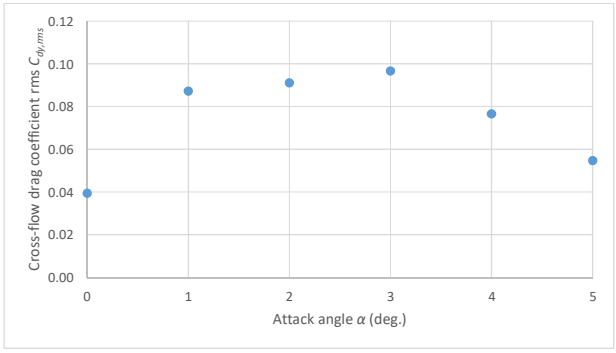


Fig. 10. Root-mean-square variation of cross-flow drag coefficient $C_{dy,rms}$ for different attack angles $\alpha$.

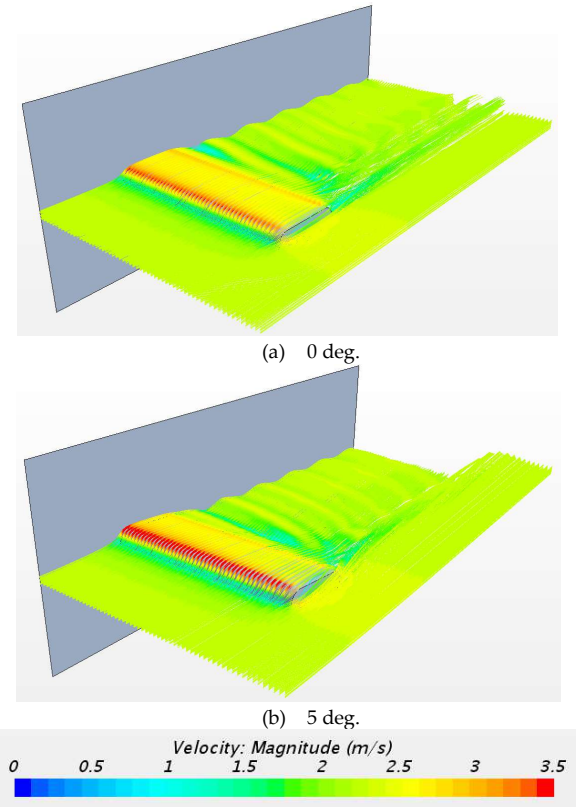


(a) 0 deg.

(b) 5 deg.

Fig. 11. Perspective view with velocity magnitude colour contour streamlines showing downstream oscillatory flow behaviour for the two attack angle variation extremes.

Vortex shedding behaviour can be more clearly seen in Figure 12 showing the side view of vorticity field at the symmetry plane. There is a clear von Karman vortex street downstream of the bluff body. There is again no perceptible difference in vorticity behavior for different $\alpha$ angles. This means for the TidGen's operational range the main elongated cylindrical form presents a risk of VIV propensity across all operational pitch angles.

Figure 13 is the vorticity field slice from a top-down view. The end region of the bluff body edge mitigates VIV to an extent. However, regular vortex shedding still occurs along the majority of the bluff body and further consideration is required to determine whether this concern is valid for the TidGen 2.0 buoyancy assembly.

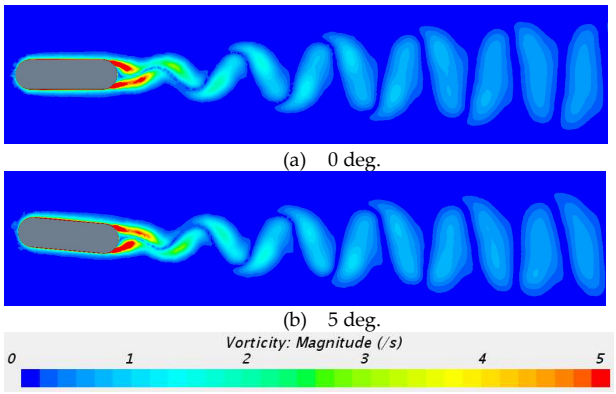


(a) 0 deg.

(b) 5 deg.

Fig. 12. Vorticity field side view for the two attack angle variation extremes.

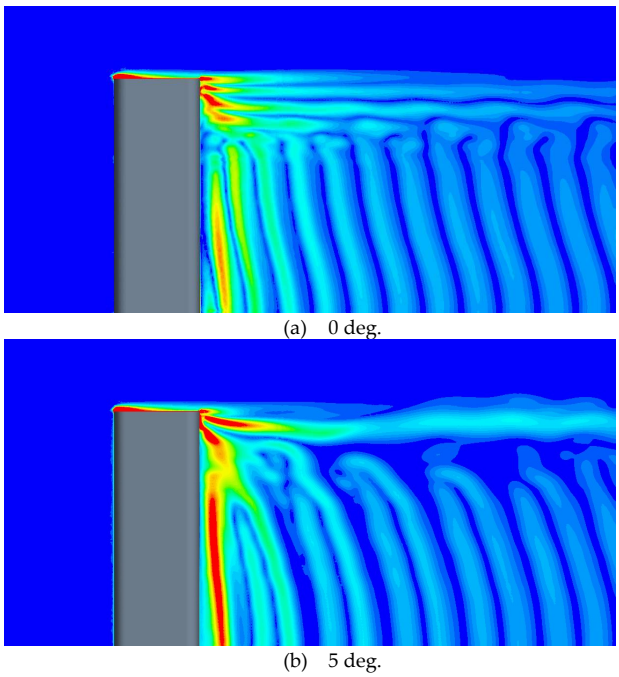

(a) 0 deg.

(b) 5 deg.

Fig. 13. Vorticity field top view for the attack angle variation extremes.

### G. *Detailed Buoyancy Assembly Geometry Hydrodynamic Characteristics*

The simplified geometry model shows that drag is consistently low but there is a risk of VIV. A further simulation is performed using the detailed geometry as shown in Figure 4 to determine if VIV is of concern to the actual TidGen buoyancy assembly. The simulation was performed at the same operational flow speed and $\alpha$ = 0 deg. angle.

Figure 14 shows the detailed geometry's vorticity field side and top views. With the side view, it can be seen the downstream flow field is significantly dissipated. There is also a less uniform flow pattern along the buoyancy component length when looking from the top view.

Table IV shows the comparison between the simplified and detailed geometry cases at $\alpha$ = 0 deg. angle. There is an increase of $C_{dx,avg}$ for the detailed geometry due to the additional surface features present which is reasonable. The $C_{dy,avg}$ approximate zero and any deviation is due to numerical error. The VIV risk considering the detailed geometry is assessed to be mitigated with $C_{dy,rms}$ reducing to 0.004. This is due to the additional surface features disrupting the regular flow pattern and having a dissipative effect on the downstream vortices.

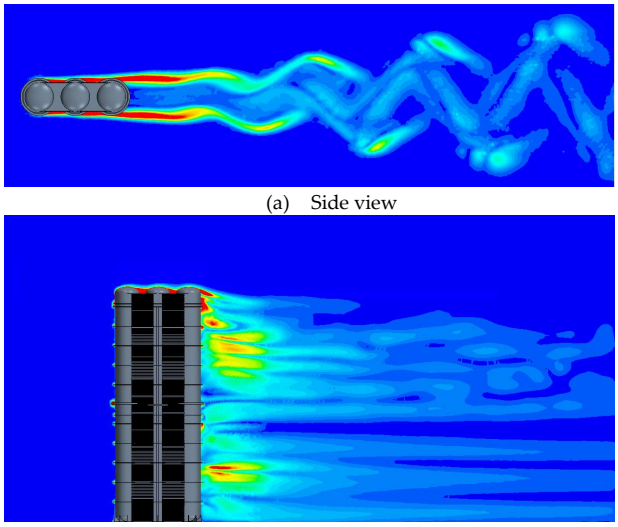

(a) Side view

(b) Top view

Fig. 14. Vorticity field for the detailed TidGen 2.0 buoyancy assembly at $\alpha$ = 0 deg.

TABLE IV
HYDRODYNAMIC CHARACTERISTIC COMPARISON BETWEEN THE SIMPLIFIED AND DETAILED BUOYANCY GEOMETRIES

| Parameters | Coefficient Magnitude | |
|---|---|---|
| | Simplified Geometry | Detailed Geometry |
| $C_{dx,avg}$ | 0.28 | 0.36 |
| $C_{dy,avg}$ | 0.01 | -0.02 |
| $C_{dy,rms}$ | 0.04 | 0.004 |

## V. CONCLUSION

The hydrodynamic performance of the buoyancy assembly for the TidGen 2.0 tidal energy harnessing system was analysed using 3-d transient computational fluid dynamics with a Reynolds-averaged Navier-Stokes approach. The buoyancy assembly can be represented in a simplified form as an elongated cylinder shape. This was the basis of the simulation which showed in-line drag to be low at about $C_{dx}$ = 0.30. The simplified geometry model also showed some risk of VIV due to the mainly uniform cylindrical shape. However a more detailed simulation of the actual TidGen buoyancy assembly with surface features such as flanges and corrugated surfaces showed the indicators of VIV risk was significantly reduced. The comparison showed the simplified geometry model to be satisfactory and conservative in representing the drag behaviour. Given the inherent possibility of VIV due to the general elongated cylinder shape, any design variation from the detailed geometry that is evaluated in this study may result in VIV and is subject to further assessment. However for the current buoyancy assembly design, it has been shown the hydrodynamic drag loading to be suitably low and there were no major concerns of VIV propensity.

## REFERENCES

[1] F. Billard and D. Laurence, "A robust k−ε-v2/k elliptic blending turbulence model applied to near-wall, separated and buoyant flows," *International Journal of Heat and Fluid Flow*, vol. 33, no. 1, pp. 45-58, February 2012.

[2] *Recommended practice: Environmental conditions and environmental loads*, DNV-RPC205, April 2014.

[3] L. S. H. Lai, "VIV-mitigating buoyancy module performance characterization using computational fluid dynamics" in *Offshore Technology Conference*, Houston, Texas, USA, 2018.